Renewable Energy 86 (2016) 280–291

Contents lists available at ScienceDirect

Renewable Energy

journal homepage: www.elsevier.com/locate/renene

Design of an efficient small wind-energy conversion system with an adaptive sensorless MPPT strategy

René Aubrée [a, b, *], François Auger [a, *], Michel Macé [c], Luc Loron [a]

[a] LUNAM University, IREENA, Saint-Nazaire, France
[b] LUNAM University, Icam, Nantes, France
[c] Fondation Ocean Vital, 9, Avenue Marcel Dassault, ZI des Fruchardières, 85340 Olonne-sur-Mer, France

ARTICLE INFO

Article history:
Received 31 January 2014
Received in revised form
29 July 2015
Accepted 30 July 2015
Available online xxx

Keywords:
Small wind turbines
Permanent magnet synchronous generator
MPPT
Angle tracking observer
Field oriented control
Extremum seeking

ABSTRACT

This paper presents an original method for the sensorless Maximum Power Point Tracking (MPPT) of a small power wind turbine using a permanent magnet synchronous generator (PMSG) to supply a DC load. This method does neither require to measure the wind speed nor to know the turbine parameters. After a presentation of the energy conversion chain (wind turbine and PMSG), we first derive an analysis of its energy efficiency. This analysis shows that the highest power at the output of the turbine and the highest power supplied to the load are not obtained at the same rotor speed. This clearly shows the interest to maximize the power supplied to the load rather than to track the maximum power at the output of the turbine deduced from its theoretical power coefficient C_p, and the interest to use an active three-phase rectifier combined with a field oriented control of the PMSG. We then describe the proposed MPPT process and the speed estimator used to design a sensorless MPPT. Simulation results demonstrate the feasibility of the proposed approach.

1. Introduction

For centuries, man converts wind into mechanical energy for its own needs. This is especially true today with the depletion of fossil fuels and the emergence of environmental issues. Large wind turbines, which are becoming more and more efficient, are now widespread. They are grouped into large wind farms and are connected to a grid. On the other hand, there is also a need for small wind turbines (SWTs), designed to produce energy in proximity to its consumer (remote sites, “off-grid” homes, relocatable equipment buildings, road signs, street lighting …) [1,2]. The optimal operation of a SWT is a key issue [3], because of its low efficiency and of its high initial cost [4]. SWTs are often specified and optimized for large wind speeds, although they mainly work at medium wind speeds. Their efficiency is therefore of primary importance, so as to harvest as much power as possible at low wind speeds [5]. As shown in Ref. [6], the efficiency of a SWT depends on many factors. One of them is the power converter. For economic reasons, low-cost power converters are usually integrated, leading to a poor efficiency which deteriorates the acceptability of SWTs. Another factor is the electric power generator. Compared to other possible generators, permanent magnet synchronous generators (PMSGs) have a higher efficiency, as the copper losses in the rotor are low, and have a larger energy density. Moreover, PMSGs may be used at low varying speeds, allowing the generator to be directly coupled to the wind turbine, without using a gearbox which would decrease the availability of the system, increase its weight and its need for maintenance [7]. However, since PMSGs are AC machines, a controlled AC/DC converter is necessary to efficiently supply a DC load. The last factors are the operating conditions. High power horizontal axis wind turbines, which are located at an altitude where the wind is slowly varying, are controlled by powerful computers with all the necessary sensors. On the other hand, SWTs are usually installed at a low height (below 12 m). At this altitude, the wind is often quickly varying in both direction and strength [8]. Low-cost small wind turbines must therefore be controlled by inexpensive microcontrollers which must perform complex algorithms to always get the maximum efficiency of the system [9]. Unfortunately, as clearly explained in Ref. [10], the maximum power point tracking (MPPT) algorithms designed for photovoltaic systems, such as the hill climbing algorithms, do not perform well

* Corresponding authors. LUNAM University, IREENA, Saint-Nazaire, France.
E-mail addresses: rene.aubree@icam.fr (R. Aubrée), francois.auger@univ-nantes.fr (F. Auger), m2.mace@sfr.fr (M. Macé), luc.loron@univ-nantes.fr (L. Loron).

http://dx.doi.org/10.1016/j.renene.2015.07.091
0960-1481/

when applied to SWTs. They can go in the wrong direction, oscillate or stall the turbine. Moreover, to decrease the cost and the encumbrance of the generator, and to increase the system reliability [11], one may wish that these control algorithms do not require any mechanical sensor [12].

The aim of this paper is to present a new sensorless algorithm that can provide the highest power to a DC load. To this aim, the studied energy conversion chain is introduced in Sections 2.1 and 2.2. Section 2.3 then presents an analysis of the performance of this chain. Two AC/DC converters are presented in Section 3. The motivations and basic principles of the Field-oriented control of a PMSG are then briefly presented in Section 4.1. The proposed MPPT algorithm and the speed estimator used to provide a sensorless algorithm are presented in Sections 4.2 and 4.3 respectively. Simulation results are finally presented in Section 5 to demonstrate the feasibility of the proposed approach.

This article extends and upgrades some elements already published in Ref. [13], in which only the content of §2 and §3.1 was presented.

2. The energy conversion chain

The wind energy conversion system studied here is made of a turbine, a direct coupled permanent magnet synchronous generator and an AC/DC converter.

2.1. The turbine

Although the approach presented in this paper could be applied to any kind of turbine, we have considered here the use of a Darrieus vertical axis wind turbine of radius R and height H. The mechanical power P_t supplied by this turbine to the generator can be expressed as [14] [15],:

$$P_t = C_p(\lambda)P_w, \quad \text{with} \quad P_w = \frac{1}{2}\rho A V_w^3 \tag{1}$$

where P_w is the power supplied by the wind (W), $A = R\,H$ is the area of the turbine (m^2), V_w is the wind speed (m/s) and ρ is the air density (around 1.2 kg/m^3 in the usual conditions of temperature and humidity). C_p is the power coefficient of the turbine, and $\lambda = R\,\Omega_m/V_w$ is the so-called tip speed ratio [1,16], Ω_m being the turbine shaft speed (rad/s). This power coefficient can be considered as a coefficient of performance and has a highly concentrated bell shape (see Fig. 1). As a consequence, due to variations in wind speed and air density, the turbine speed must permanently be adjusted by a maximum power point tracking algorithm, to provide the greatest power to the load [8,17].

2.2. The permanent magnet synchronous generator

To accurately reproduce its behavior during transients, we use a dynamic model of the PMSG, expressed in the Park (dq) reference frame rotating at the same speed as the rotor. If the stator windings are supposed to be sinusoidally distributed, if the magnetic circuits are supposed to be unsaturated and if the eddy currents and hysteresis losses are supposed to be negligible, the electrical equations expressed in this frame using the Concordia transform [18,15], are (see Fig. 2)

$$v_d = -R_s\, i_d - \omega_e\, \Psi_q + \frac{d\Psi_d}{dt} \tag{2}$$

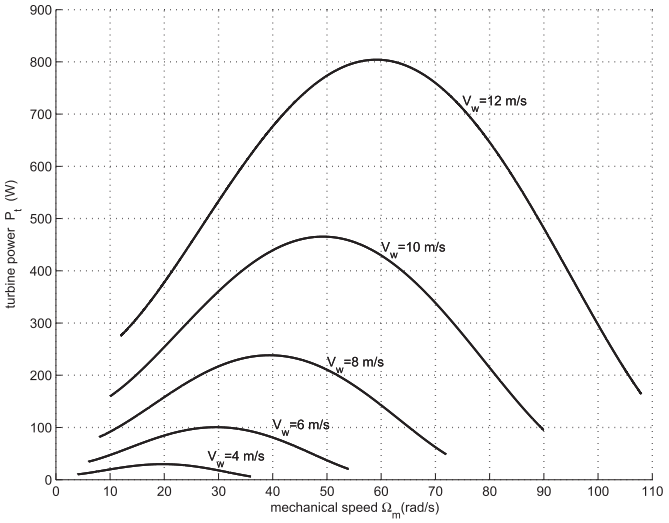

Fig. 1. Turbine power P_t vs the turbine rotation speed Ω_m for different values of the wind speed V_w and a constant value of the air density (ρ = 1.2 kg/m^3). The power coefficient has been approximated by a fourth-order polynomial deduced from experimental measurements.

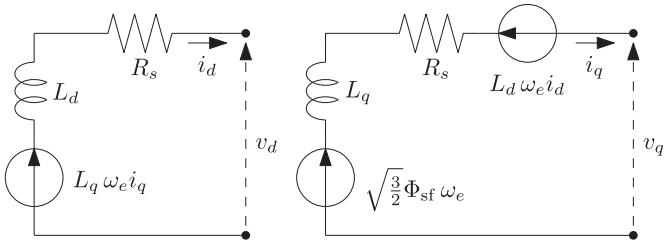

Fig. 2. Equivalent electrical model of a PMSG.

$$= -R_s\, i_d + L_q\, \omega_e\, i_q - L_d\frac{di_d}{dt} + e_d \tag{3}$$

$$v_q = -R_s\, i_q + \omega_e\, \Psi_d + \frac{d\Psi_q}{dt} \tag{4}$$

$$= -R_s\, i_q - L_d\, \omega_e\, i_d - L_q\frac{di_q}{dt} + e_q \tag{5}$$

where $e_d = 0$ V and $e_q = \sqrt{3/2}\Phi_{sf}\,\omega_e$ are the no-load voltages (obtained when $i_d = i_q = 0$ A), R_s is the stator phase resistance, L_d and L_q are the dq inductances, ω_e is the angular frequency of the electric voltages and currents, Φ_{sf} is the rotor flux linkage, $\Psi_d = -L_d\, i_d + \sqrt{3/2}\Phi_{sf}$ and $\Psi_q = -L_q\, i_q$ the d-q axis magnetic fluxes. For a synchronous machine, $\omega_e = p\,\Omega_m$, p being the pole pairs number. The production of this electric energy at the output of the generator induces a braking electromagnetic torque. The general expression of this torque is:

$$T_e = -p(\Psi_d\, i_q - \Psi_q\, i_d) \tag{6}$$

$$= -p\left(\sqrt{\frac{3}{2}}\Phi_{sf}\, i_q + (L_q - L_d) i_d\, i_q\right) \tag{7}$$

Finally, the turbine torque and the electromagnetic torque are involved in a mechanical equation [19].

$$J\frac{d\Omega_m}{dt} = T_t + T_e - f\Omega_m \tag{8}$$

where J is the overall system inertia, f is the viscous friction coefficient and $T_t = P_t/\Omega_m$ is the torque provided by the wind turbine.

2.3. Energy efficiency analysis

When considering an energy conversion system, it may be interesting to study its energy efficiency. This requires computing the power supplied at the output of the three-phase generator

$$P_g = v_a\, i_a + v_b\, i_b + v_c\, i_c = v_d\, i_d + v_q\, i_q \tag{9}$$

From Eqs. (3), (5) and (7), one can deduce that:

$$P_g = -R_s\left(i_d^2 + i_q^2\right) - \frac{1}{2}\left(L_d\frac{di_d^2}{dt} + L_q\frac{di_q^2}{dt}\right) - T_e\Omega_m \tag{10}$$

At steady state, $di_d/dt = di_q/d\,t = 0$ A/s and $d\Omega_m/d\,t = 0$ rad/s^2, so the power equals the difference between the power supplied by the turbine and the Joule and friction losses:

$$P_g = C_p\left(\frac{R\Omega_m}{V_w}\right)P_w - R_s\left(i_d^2 + i_q^2\right) - f\Omega_m^2, \quad \text{with} \tag{11}$$

$$C_p\left(\frac{R\Omega_m}{V_w}\right)P_w - f\Omega_m^2 = -T_e\,\Omega_m \tag{12}$$

To maximize P_g subject to the constraint given by Eq. (12), we can use the method of Lagrange multipliers [20]. This consists in defining the Lagrange function

$$\mathscr{L} = P_g + \lambda_{\mathscr{L}}\left[C_p\left(\frac{R\Omega_m}{V_w}\right)P_w - f\Omega_m^2 + T_e\,\Omega_m\right] \tag{13}$$

and to look for a stationary point of this function, i.e. for a solution of the four equations

$$\frac{\partial\mathscr{L}}{\partial i_d} = 0, \quad \frac{\partial\mathscr{L}}{\partial i_q} = 0, \quad \frac{\partial\mathscr{L}}{\partial\Omega_m} = 0 \quad \text{and} \quad \frac{\partial\mathscr{L}}{\partial\lambda_{\mathscr{L}}} = 0 \tag{14}$$

A summary of the solution of this optimization problem is that.

- In steady state,

$$i_d = \sqrt{\frac{3}{2}}\,\frac{\lambda_{\mathscr{L}}^2(L_q - L_d)p^2\,\Omega_m^2\,\Phi_{sf}}{4R_s^2 - \lambda_{\mathscr{L}}^2(L_q - L_d)^2p^2\,\Omega_m^2} \tag{15}$$

$$\text{and} \quad i_q = \frac{C_p\left(\frac{R\Omega_m}{V_w}\right)P_w - f\Omega_m^2}{\sqrt{\frac{3}{2}}p\,\Phi_{sf}\,\Omega_m + (L_q - L_d)p\,\Omega_m\,i_d} \tag{16}$$

- For a non salient machine ($L_q = L_d$) such as the one we consider, P_g is maximized when $i_d = 0$ A. This justifies the use of a controlled rectifier based on the field oriented control principle.
- P_g is then maximized when Ω_m is the solution of the nonlinear equation

$$(\lambda_{\mathscr{L}} + 1)\frac{R\Omega_m}{V_w}\frac{dC_p}{d\lambda}\left(\frac{R\Omega_m}{V_w}\right) = \lambda_{\mathscr{L}}C_p\left(\frac{R\Omega_m}{V_w}\right) + (\lambda_{\mathscr{L}} + 2)\frac{f\Omega_m^2}{P_w} \tag{17}$$

$$\text{with} \quad \lambda_{\mathscr{L}} = \frac{4R_s}{3p^2\,\Phi_{sf}^2}\left(f - \frac{P_w}{\Omega_m^2}C_p\left(\frac{R\Omega_m}{V_w}\right)\right) \tag{18}$$

One can check that when $R_s = 0\,\Omega$, $\lambda_{\mathscr{L}}$=0, and if f also equals zero, then Ω_m is deduced from the location of the maximum of $C_p(R\Omega_m/V_w)$. This analysis allows one to define the optimal generator power coefficient as

$$C_{ogp}(\Omega_m, V_w) = \frac{P_g}{P_w} = C_p\left(\frac{R\Omega_m}{V_w}\right) - \frac{R_s i_q^2 + f\Omega_m^2}{P_w}, \tag{19}$$

where i_q is given by Eq. (16). This coefficient evaluates the efficiency of the association of a wind turbine with a PMSG optimally controlled by the field oriented vector control principle, and the importance of the Joule and friction losses compared to the wind power. Fig. 3 shows a comparison of C_p and C_{ogp} in our case. One important point to underline is that since R_s and f are not zero, these two curves do not reach their maximum at the same abscissa. This means that when the value of the tip speed ratio λ for which C_p is at its maximum is used to compute the speed reference of a speed controlled generator, the highest power at the output of the generator is not provided. This justifies to directly maximize the power supplied to the load.

3. The AC/DC conversion

To supply a DC load by the wind turbine, two AC/DC converters can be considered and compared. The first one is based on the use of a standard diode bridge rectifier, and the second one is made of 6 power switches driven by field oriented control. In both cases, step-up converters are used to optimally control the turbine speed through the DC current i_{dc}. To charge a battery, these structures may be followed by another power converter, which is out of the scope of this paper.

3.1. The diode-based AC/DC converter

The least expensive solution is probably an AC/DC converter made of a 3-phase diode bridge associated with a boost circuit (see Fig. 4). A boost circuit [21] is a step-up chopper made of L_1, T_1 and

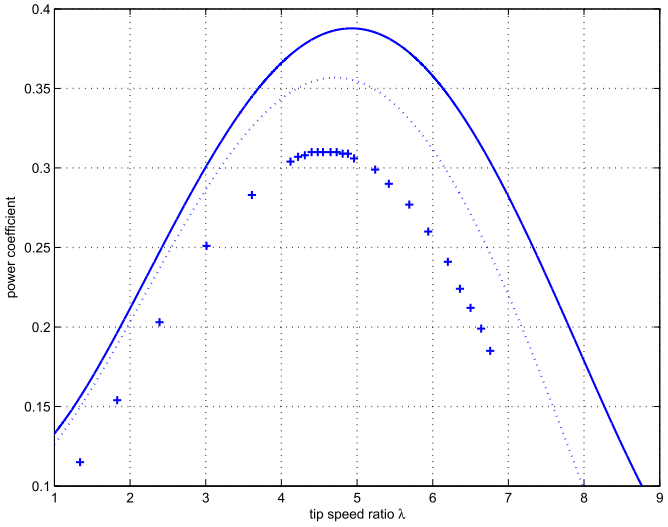

Fig. 3. Power coefficient of the turbine C_p (continuous line), optimal generator power coefficient C_{ogp} (dotted lines) and power coefficient obtained with the diode-based AC/DC converter considered in Section 3.1 (cross mark) vs the tip speed ratio $\lambda = R\Omega_m/V_w$. C_{ogp} is computed for $V_w = 6$ m/s, with the model parameters given in appendix.

D_7. It converts the output voltage of the diode bridge v_{in} into the load voltage v_{dc} (see Fig. 4). It is driven by the periodic pulse width modulation (PWM) signal which controls the power switch T_1 and hence the amount of power transferred to the load. Indeed, if the boost circuit is used in continuous mode, the current across the inductance never reaches zero and is a periodic piecewise linear signal, varying between a minimum i_{min} and a maximum i_{max}. When the switch is on (see Fig. 5), the current increases up to

$$i_{max} = i_{min} + v_{in}\, T_{on}/L \tag{20}$$

where T_{on} is the on-state time of the switch. When the switch is off, the current decreases down to

$$i_{min} = i_{max} - (v_{dc} - v_{in})(T - T_{on})/L \tag{21}$$

where T is the period of the PWM signal. From Eqs. 20 and 21, one can deduce that [16].

$$v_{dc} = \frac{1}{1-D} v_{in} \tag{22}$$

where $D = T_{on}/T$ is the duty cycle of the PWM signal. This means that the power supplied to the load (R_L) is

$$P_L = \frac{v_{dc}^2}{R_L} = \frac{v_{in}^2}{(1-D)^2 R_L} \tag{23}$$

This result shows that for the diode bridge, the boost circuit can be considered as a variable resistive load with an equivalent value $R_{eq} = (1-D)^2 R_L$. Since this equivalent resistance determines the current supplied by the generator and hence the rotor speed, the duty cycle D can be used to maximize the power supplied to the load. A second advantage of this structure is therefore to control the power provided by the PMSG by a single PWM signal. But obviously, this does not allow a separate control i_d and i_q, and thus an extraction of the maximum power of the generator, as shown in Fig. 3. But the initial cost reduction may compensate this. Moreover, because of the diode commutations, only two phases of the generator are active at the same time. This circuit also generates a current variation $i_{max} - i_{min} = v_{in} TD/L$ that can be limited by an appropriate choice of the inductance and of the PWM frequency.

3.2. The actively-controlled-switch-based AC/DC converter

A more expensive but more efficient AC/DC converter [22] is made of an active three-phase rectifier using six power switches controlled by PWM signals (see Fig. 6). This step-up converter is called a boost converter [23]. Each leg of the inverter is connected to a line inductance and acts as a boost circuit, the current being returned to the PMSG by one of the other two legs, depending on the phase voltages. Since the legs are driven by three independent PWM signals, the phase currents can be controlled separately,

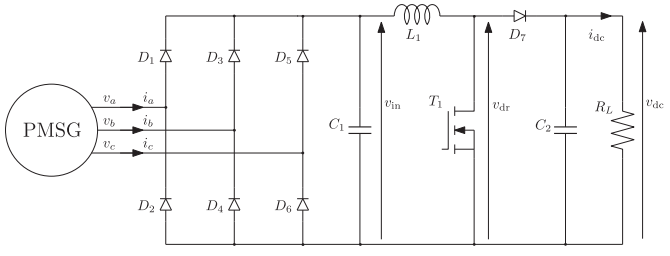

Fig. 4. AC/DC converter obtained by a diode bridge rectifier associated with a boost circuit.

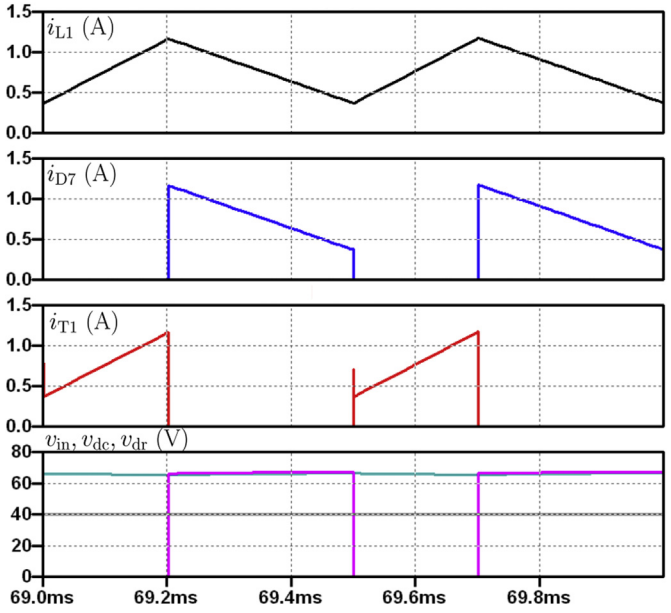

Fig. 5. Currents and voltages inside a simulated boost circuit. From top to bottom: current across the inductance, current across the switch, current across the diode and voltages v_{in} (gray), v_{dc} (green) and v_{dr} (violet). Since $v_{in} = 40$ V, $v_{dc} = 66$ V, $T = 0.5$ ms and $T_{on} = 0.2$ ms ($D = 0.4$), Eq. (22) is satisfied. (For interpretation of the references to color in this figure legend, the reader is referred to the web version of this article.)

allowing a maximum power extraction from the PMSG thanks to a field oriented control [24].

If the voltages and currents of the PMSG are supposed to be well-balanced and if s_a, s_b, s_c denote the switching functions of the power switches (T_1 is on when $s_a = 1$ and T_2 is on when $s_a = 0$), then this converter can be modelized as a state-space system

$$L_{li}\frac{di_a}{dt} = -R_{li}\, i_a - \frac{2s_a - s_b - s_c}{3} v_{dc} + v_a \tag{24}$$

$$L_{li}\frac{di_b}{dt} = -R_{li}\, i_b - \frac{2s_b - s_a - s_c}{3} v_{dc} + v_b \tag{25}$$

$$C\frac{dv_{dc}}{dt} = (s_a - s_c) i_a + (s_b - s_c) i_b - \frac{v_{dc}}{R_L} \tag{26}$$

where R_{li} is the resistance of the line inductances (combined with the resistance of the current sensors). Such a model allows for an accurate simulation, as well as for a low frequency approximation through the use of the generalized state-space averaging approach [6].

4. The system control

4.1. The field oriented control

The field oriented control [25,26], also called vector control, achieves under all operating conditions a torque control of the PMSG that minimizes the power losses and can be compared to that of a DC generator. It involves forcing the i_d current to be zero thanks to an active three-phase rectifier, so that the electromagnetic torque can be easily controlled by i_q: Eq. (6) shows that if $i_d = 0$ A, then $T_e = -\sqrt{\frac{3}{2}} p\, \Phi_{sf}\, i_q$.

We chose an indirect control, which means that the fluxes are not measured, but simply deduced from the measured currents and from the model parameters. From Eqs. (3) and (5) and from Fig. 6,

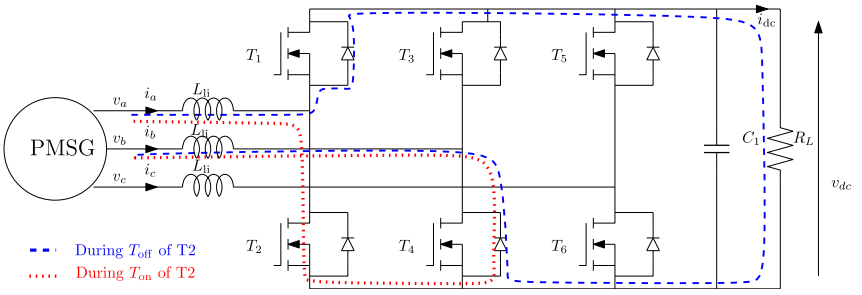

Fig. 6. The controlled rectifier. When $v_a > v_c > v_b$, the current flows through T_4 when T_2 (dotted lines) or T_1 (dashed lines) is closed.

one can show that i_d and i_q can be independently controlled through two voltages v_{d1} and v_{q1}:

$$v_{d1} = v_d + \omega_e \Psi_q = v_d - L_q\, \omega_e\, i_q = -(L_d + L_{li})\frac{di_d}{dt} - (R_s + R_{li})i_d \tag{27}$$

$$v_{q1} = v_q - \omega_e \Psi_d = v_q + L_d\, \omega_e\, i_d - \sqrt{3/2}\, \Phi_{sf}\, \omega_e$$
$$= -(L_q + L_{li})\frac{di_q}{dt} - (R_s + R_{li})i_q, \tag{28}$$

Thus, the basic principle of the field oriented control is as illustrated on Fig. 7. First, a Park transform [27] is applied to the measured line currents i_a, i_b, i_c, to provide i_d and i_q. Two current controllers are then used to determine the voltages v_{d1} and v_{q1} that should be used to obtain the desired current references i_{dref} and i_{qref}. The dq voltages are then deduced from v_{d1} and v_{q1} by decoupling relations

$$v_d = v_{d1} + L_q\, \omega_e\, i_q \tag{29}$$

$$v_q = v_{q1} - L_d\, \omega_e\, i_d + \sqrt{3/2}\, \Phi_{sf}\, \omega_e \tag{30}$$

An inverse Park transform is finally used to compute the duty cycles of the three legs of the active rectifier.

For the control of i_d and i_q, we chose two IP controllers (see Fig. 8), which are PI controllers relocating the proportional action from the direct path into the feedback loop [28], allowing to avoid overshoots on the output voltage during the transients. Since the expected performances and the model parameters are the same for i_d and i_q, both controllers are tuned identically. From Fig. 8, one can deduce that

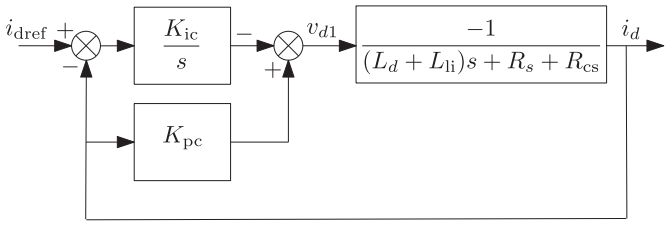

Fig. 8. Block diagram of the i_d current controlled by an IP controller. The i_q current is controlled in exactly the same way.

$$I_d = \frac{-1}{(L_d + L_{li})s + R_s + R_{cs}}\left(K_{pc} I_d - \frac{K_{ic}}{s}\left(I_{dref} - I_d\right)\right) \tag{31}$$

$$= \frac{1}{\frac{(L_d + L_{li})}{K_{ic}}s^2 + \frac{K_{pc} + R_s + R_{cs}}{K_{ic}}s + 1} I_{dref} \tag{32}$$

$$= \frac{1}{\frac{s^2}{\omega_n^2} + 2\xi\frac{s}{\omega_n} + 1} I_{dref} \tag{33}$$

where K_{pc} and K_{ic} are the proportional and integral coefficients of the IP current controller, I_d and I_{dref} are the Laplace transforms of i_d and i_{dref} and s is the Laplace variable. Eq. (32) shows that the transfer function between I_{dref} and I_d is a second-order allpole transfer function of unit static gain, that can be written in its canonical form with a natural angular frequency $\omega_n = \sqrt{K_{ic}/(L_d + L_{li})}$ and a damping ratio $\xi = (K_{pc} + R_s + R_{cs})/2\sqrt{K_{ic}(L_d + L_{li})}$. Among all the possible ways to tune the controller parameters, we chose to deduce them from a desired damping ratio ξ and a desired angular frequency bandwidth ω_c:

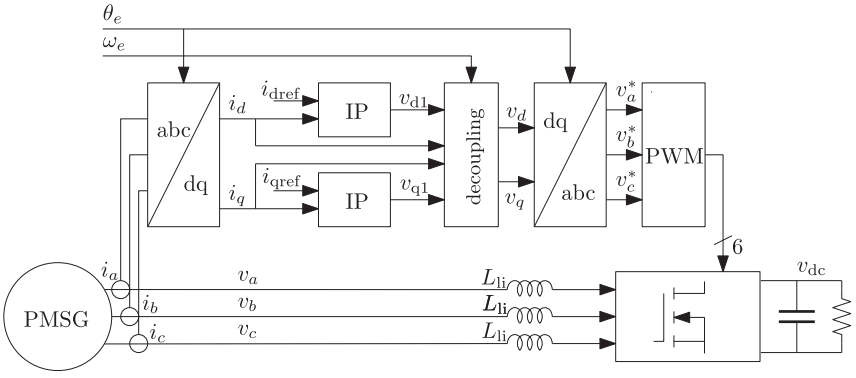

Fig. 7. Field oriented control structure.

$$K_{pc} = 2\xi\omega_n(L_d + L_{li}) - R_s - R_{cs} \tag{34}$$

$$K_{ic} = (L_d + L_{li})\omega_n^2 \tag{35}$$

$$\text{with } \omega_n = \omega_c\sqrt{2\xi^2 - 1 + \sqrt{\left(2\xi^2 - 1\right)^2 + 1}} \tag{36}$$

For the system parameters given in Appendix, for $\xi = 2$ (to avoid overshoots) and $f_c = \omega_c/(2\pi)$=10 Hz, we obtain $K_{pc} = 16.6\,\Omega$ and $K_{ic} = 1000\,\Omega/s^{-1}$.

4.2. The maximum power point tracker

As shown in Section 3.1, using a diode-based AC/DC converter allows to control the power provided to the load through the duty cycle D. In Section 4.1, we showed that this power can also be controlled through the i_q current when a switch-based AC/DC converter driven by vector control is used. Both variables D and i_q can therefore be derived from the same power maximization process. We designed a continuous-time maximum power point tracker which can be compared to the discrete-time MPPT algorithms proposed in Refs. [16,12,29], and which consists of three parts:

- *a power controller.* As for the currents i_d and i_q, the load power is regulated by an IP controller (see Fig. 9). Simulations have shown that with our vector controlled PMSG, the dynamic system between i_q and P_L provides a current step response similar to a first-order system of static gain $K_o = 64$ V and a time constant $T_o = 0.11$ s. With an IP controller, the closed-loop transfer function between P_{ref} and P_L is also a second-order system

$$P_L = \frac{K_o}{1 + sT_o}\left(\frac{K_{ip}}{s}\left(P_{ref} - P_L\right) - K_{pp}P_L\right) \tag{37}$$

$$= \frac{1}{\frac{T_o}{K_oK_{ip}}s^2 + \frac{1+K_oK_{pp}}{K_oK_{ip}}s + 1}P_{ref} \tag{38}$$

If the controller parameters are once again deduced from a desired damping ratio ξ and a desired angular frequency bandwidth ω_c, then

$$K_{pp} = \frac{2\xi\omega_nT_o - 1}{K_o} \quad \text{and} \quad K_{ip} = \frac{\omega_n^2T_o}{K_o}, \tag{39}$$

ω_n being deduced from ω_c by Eq. (36). For example, for $\xi = \sqrt{2}/2$ and $f_c = \omega_c/(2\pi)$=10 Hz, we obtain $K_{pp} = 0.12\,V^{-1}$ and $K_{ip} = 6.17\,V^{-1}\,s^{-1}$.

- *a power reference generator.* From Eq. (1), one can show [2,30] that the maximum value of P_t is a cubic function of the rotor speed Ω_m:

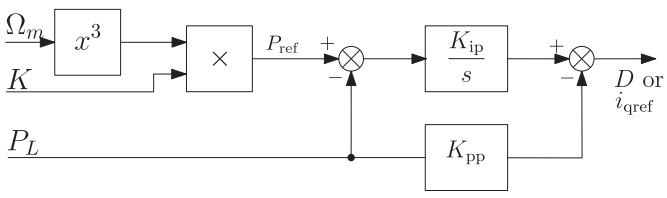

Fig. 9. The power reference generator and power regulation loop.

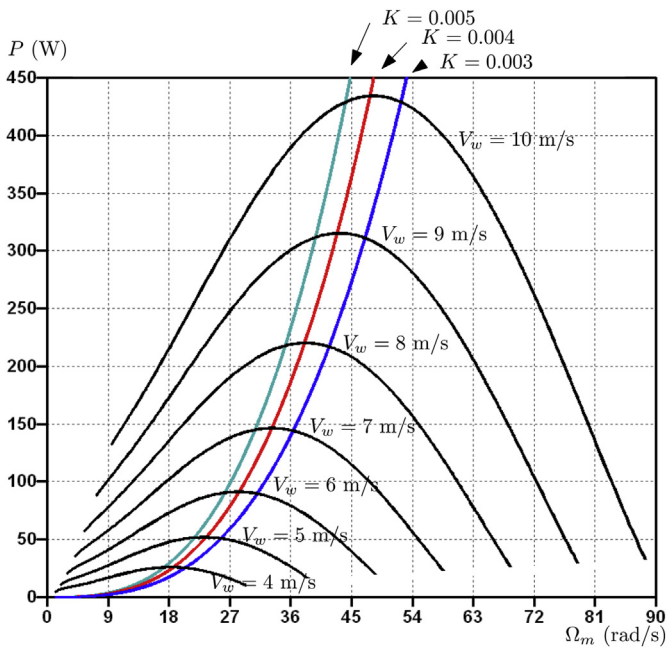

Fig. 10. Load power P_L as a function of the rotor speed Ω_m for a constant wind speed ranging from 4 to 10 m/s. The maxima of these curves can be compared to cubic curves $K\,\Omega_m^3$ for three values of K.

$$P_{t\_opt} = K_{opt}\,\Omega_m^3, \quad \text{with } K_{opt} = \frac{\rho AR^3}{2\lambda_{opt}^3}C_p(\lambda_{opt}), \tag{40}$$

λ_{opt} being the tip speed ratio for which $C_p(\lambda)$ reaches its maximum. Based on the assumption that P_L behaves the same, we also chose the power reference to be a cubic function of the rotor speed: $P_{ref} = K\,\Omega_m^3$. Fig. 10 shows plots of P_L vs Ω_m for 7 values of the wind speed. This figure shows that the maxima of these plots are close to a cubic curve $K\,\Omega_m^3$, with $K \approx 4\,10^{-3}$. This figure also shows that a 25% error on K leads to a very small power loss at low wind speeds. Having an accurate value of K is important for large wind speeds only.

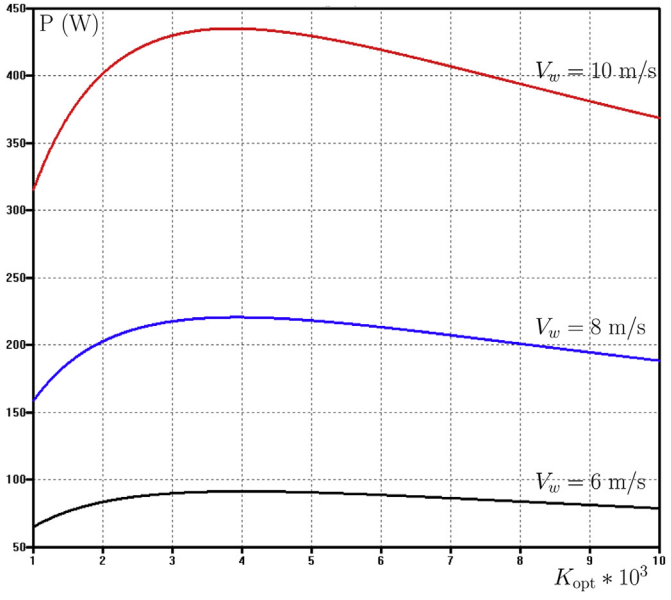

Fig. 11. Load power P_L versus K for three different constant wind speeds.

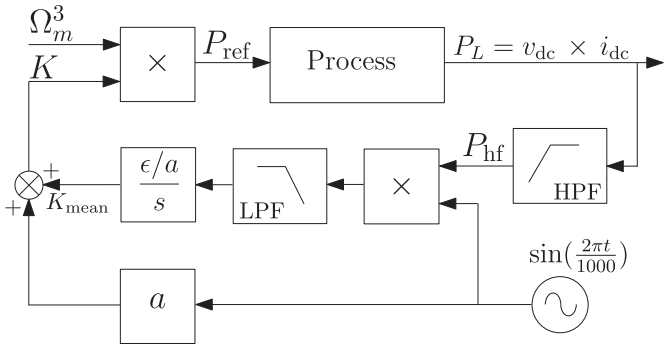

Fig. 12. Maximum seeking process used to determine *K*.

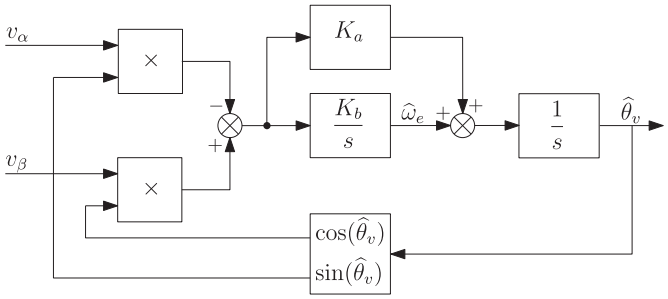

Fig. 13. Block diagram of the angle tracking observer.

- *an algorithm to track variations of climate and turbine state.* Eq. (40) shows that K_{opt} is proportional to the air density [31]. It also depends on the geometrical dimensions of the turbine. Therefore, the *K* coefficient used in the power reference generator varies with the atmospheric conditions and the distortion of the turbine. As shown in Figs. 10 and 11, when the wind speed is constant, the load power reaches a maximum for a particular value of *K*. This particular value is nearly the same for all speeds. Thus, an extremum seeking method (ESC) [32–34] is used to continuously determine the optimal value of *K*. This robust and effective method adds to this optimal value, called K_{mean} (see Fig. 12), a sinusoidal disturbance of amplitude *a*. The power variation resulting from this dither signal is extracted by a high-pass filter and demodulated by a multiplication with the dither signal. A low-pass filter is then used to keep the DC component of this product, which is proportional to the amplitude of the fundamental term of P_{hf} and which is integrated to provide K_{mean}. The gain ε determines the variation speed of K_{mean}. A study of the robustness and stability of this method can be found in Refs. [35,36].

The tuning of the algorithm parameters was done experimentally during simulations. First, the period of the dither signal is chosen greater than the response time of the wind turbine to allow the ESC to have enough time to have an influence on the power delivered by the wind turbine. In our case, for a response time of the wind turbine equal to approximately 500 s, we selected a dither period equal to 900 s. Then the amplitude *a* of the dither must be significantly large to generate wind turbine power variation which emerges from the noise and provides a good idea on the sign of this variation. We chose $a = 7\,10^{-4}$. Finally, the ε/a gain is gradually increased to accelerate the convergence of the system without degrading the energy performance at steady state. For this, we chose $\varepsilon = 7\,10^{-11}$.

4.3. The speed estimator

We tried to further reduce the initial cost of this energy conversion chain by removing the need of a speed sensor [37]. For this, we used an Angle Tracking Observer (ATO) studied in Ref. [38]. This estimator is fed by the projections of the output voltages of the generator in the fixed $\alpha\beta$ reference frame, using a Clarke transform. These projections are the coordinates of a vector rotating at the electrical rotor speed $\omega_e = p\Omega_m$. To estimate this speed, the ATO consists in making an angle $\widehat{\theta}_v$ evolve so as to cancel the algebraic area of the triangle formed by the two vectors (V_α,V_β) and $(\cos(\widehat{\theta}_v), \sin(\widehat{\theta}_v))$, which is proportional to $V_\beta \cos(\widehat{\theta}_v) - V_\alpha \sin(\widehat{\theta}_v)$. This cancellation is obtained by a classical PI controller. The resulting $\widehat{\theta}_v$ is an estimation of the angular position of the voltage vector in the fixed $\alpha\beta$ reference frame. Fig. 13 shows the block diagram of the speed and angle tracking observer.

As shown in Fig. 7, the field oriented control requires an estimation of θ_e, which is the angle between the rotating d axis and the fixed α axis. This estimation must be deduced from $\widehat{\theta}_v$. Since the PMSG is directly coupled and since the inertia of the turbine is large, the rotor speed is very slowly varying, and the vector controlled stator currents can be considered as in steady state at the mechanical time scale. Eqs. (3) and (5) then become $v_d = L_q\,\omega_e\,i_q$ and $v_q = \sqrt{3/2}\Phi_{sf}\,\omega_e - R_s\,i_q$, resulting in

$$\theta_v - \theta_e = \arctan\left(\frac{v_q}{v_d}\right) = \arctan\left(\frac{\sqrt{3/2}\,\Phi_{sf}\,\omega_e - R_s\,i_q}{L_q\,\omega_e\,i_q}\right) \qquad (41)$$

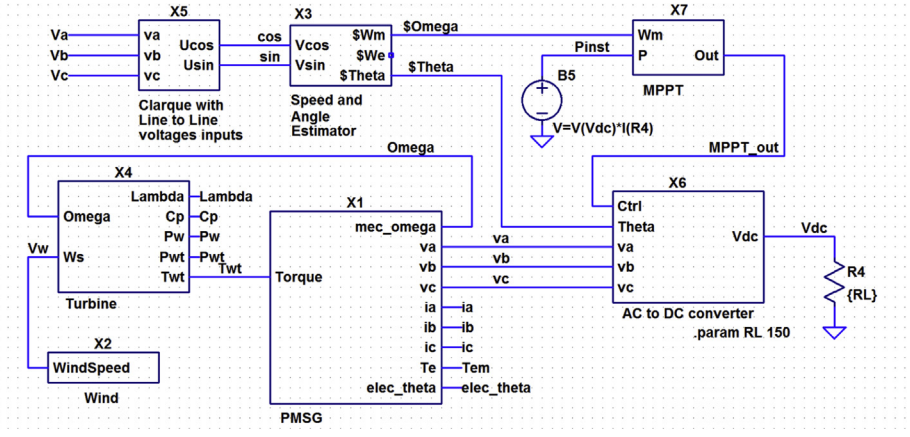

Fig. 14. Block diagram of the system simulated with LTspice.

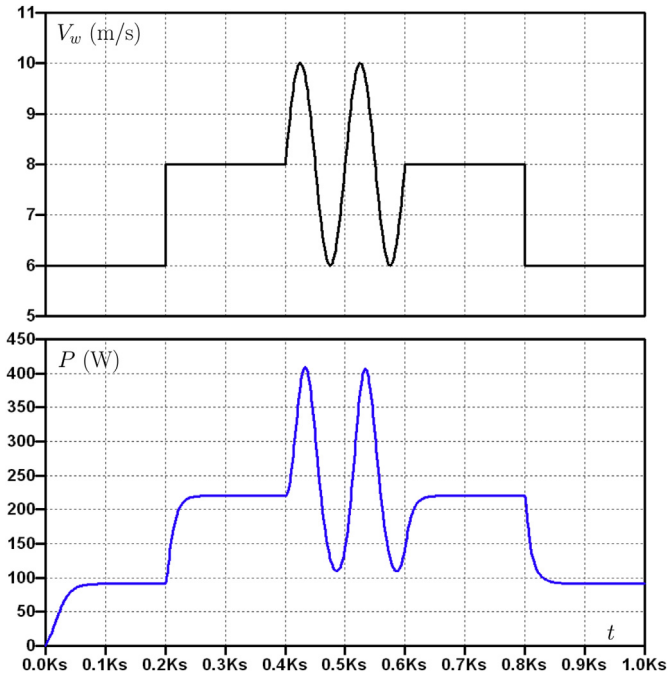

Fig. 15. Simulation results showing the power provided by the proposed system for a varying wind speed.

To avoid numerical inconvenience when i_q is close to zero, the relationship $\arctan(x)+\arctan(1/x) = \pi/2$ (for $x > 0$) is used to derive an estimator of the d axis position as

$$\widehat{\theta}_e = \widehat{\theta}_v - \frac{\pi}{2} + \arctan\left(\frac{L_q\ \widehat{\omega}_e\ i_q}{\sqrt{3/2}\Phi_{sf}\ \widehat{\omega}_e - R_s\ i_q}\right) \quad (42)$$

One can check that this expression simply reduces to $\widehat{\theta}_e = \widehat{\theta}_v - \frac{\pi}{2}$ at no-load ($i_q = 0$ A).

5. Simulation results

The performance of the proposed solution has been evaluated by numerous simulations using the general purpose free full-fledged LTspice IV software [39]. Simulations allow to compare solutions under strictly identical conditions, and we justify the choice of this software by its capacity to efficiently simulate both dynamic systems and electronic circuits such as switch-mode power supplies. The spice models provided by the component manufacturers include the non-linear phenomena of semiconductor components such as diodes and transistors. The PMSG model was built from the mathematical expressions described in §2.2. Fig. 14 shows a block diagram of the simulation system. The values of the parameters are given in Appendix. In our case, the maximum power point of the turbine is obtained for $\lambda = 4.95$ (since Darrieus turbines are lift-based, the speed of the apparent wind at the blade tip is greater than the speed of the real wind, so λ is greater than one). The setting of the ATO was performed as proposed in Ref. [38], with a damping ratio $\xi = 1.945$ and a maximum permissible error of 1°.

The proposed solution has been extensively tested with both constant and varying wind speeds. Fig. 15 shows the load power evolution when the wind speed evolution is made of steps and pieces of sinusoids. This figure illustrates the mid-term stability of the power controller included in the MPPT process. Fig. 16 shows plots of K_{mean} vs time obtained for four different initial

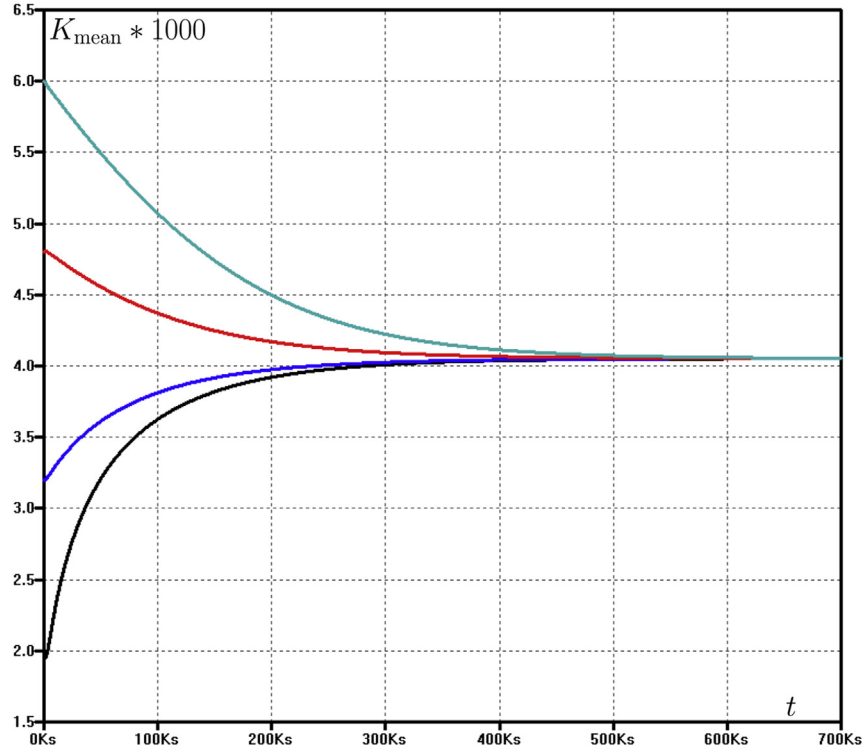

Fig. 16. Simulation results showing the evolution of K_{mean} resulting from four different initializations of the maximum seeking process used in the proposed system. The wind speed is constant, equal to 6 m/s.

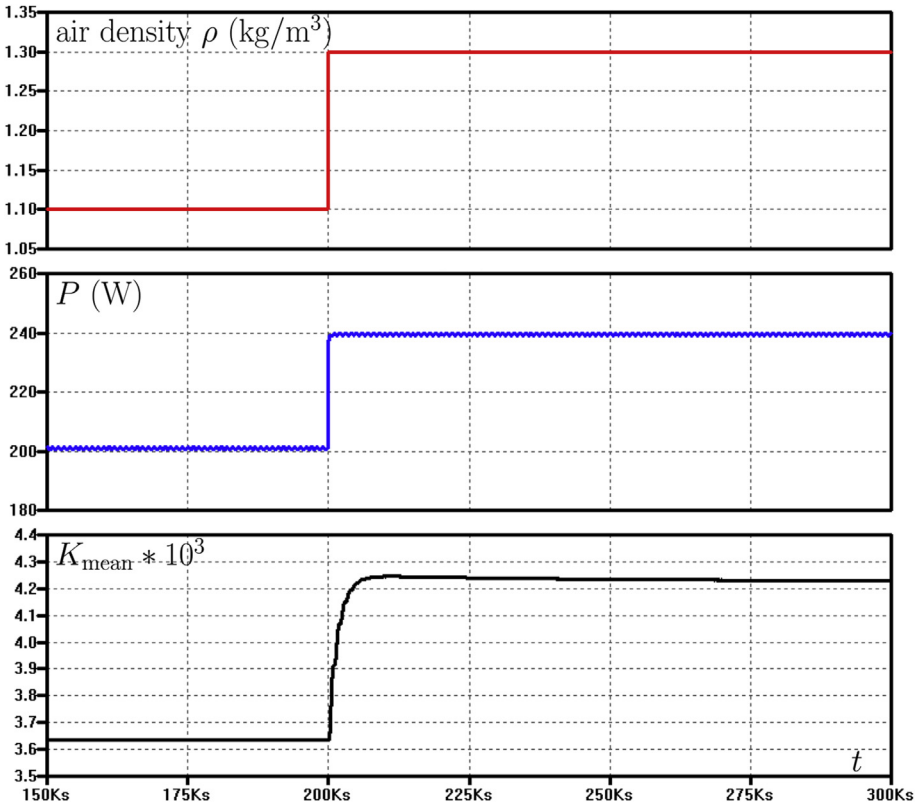

Fig. 17. Simulation results showing the evolutions of the load power and of K_{mean} resulting from an abrupt change of the air density. The wind speed is constant, equal to 8 m/s.

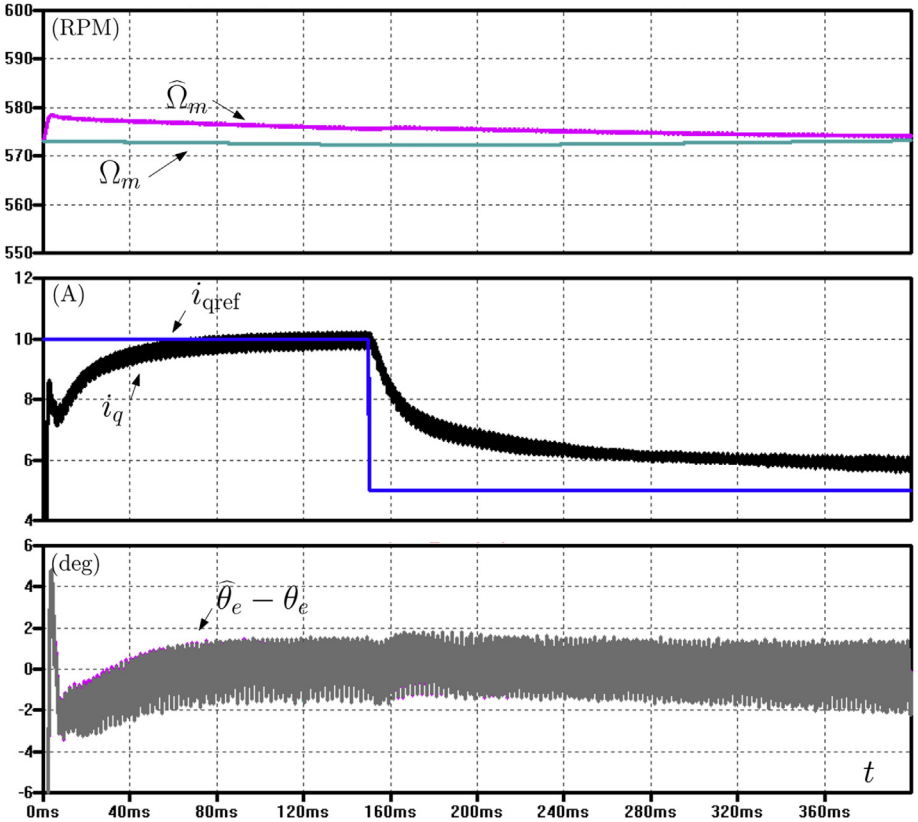

Fig. 18. Simulation results showing the convergence of the ATO at startup and after a current reference step. From top to bottom: true and estimated rotor speed, i_{q} and i_{qref} and position estimation error $\widehat{\theta}_e - \theta_e$. The wind speed is constant equal to 12 m/s. During these simulations, the values of R_s, $L_d = L_q$ and Φ_{sf} have a variation equal to ±10% around the nominal values. As the waveforms are very similar, we cannot distinguish the differences between the different steps.

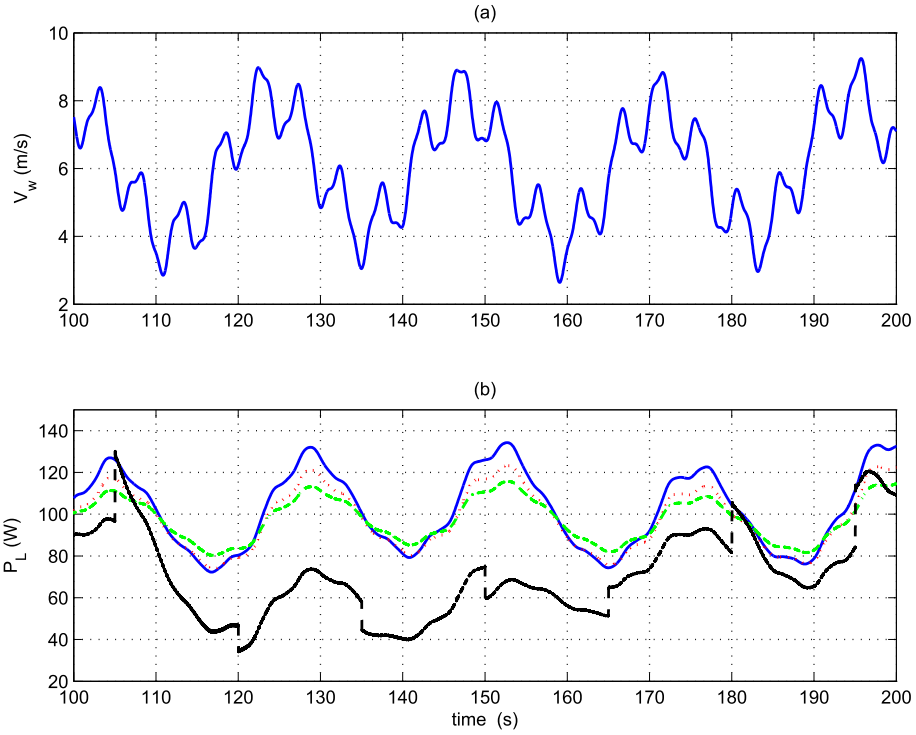

Fig. 19. Simulation results showing (a) the wind speed obtained when using a sinusoidal model [40] and (b) the resulting output power obtained when using a vector-controlled switch-based AC/DC converter (solid blue line), a diode based rectifier with a boost circuit (dotted red lines), a diode-based rectifier with a fixed resistive load ($R_L = 35\,\Omega$) fitted to an average wind speed of 6 m/s instead of the resistive load ($R_L = 150\,\Omega$) used in all the other cases (green dashdotted lines), and a diode-based rectifier with a boost circuit controlled by an empirically adjusted HCS MPPT [16,40,42] (black dashed lines). (For interpretation of the references to color in this figure legend, the reader is referred to the web version of this article.)

Table 1
Diode-based versus MLI AC/DC converter performances.

Wind speed value	Output power of the diode-based rectifier	Output power of the switch-based AC/DC converter	Relative increase of efficiency
6.0 m/s	82.5 W	91.23 W	9.6%
8.0 m/s	204.0 W	220.2 W	7.4%
10.0 m/s	409.0 W	434.0 W	5.8%

values and a constant wind speed (equal to 6 m/s). This figure illustrates that the maximum seeking process converges to the same value whatever its initialization. Fig. 17 shows the evolution of K_{mean} when the air density abruptly changes from 1.1 to 1.3 kg/m^3. This figure illustrates that the maximum seeking process converges to a correct value after 3 h. As shown in Eqs. (1) and (40), this variation approximately increases the wind power (and therefore the load power) and the value of K_{mean} by a factor 1.3/1.1. This shows that the maximum seeking algorithm eliminates the need for temperature and humidity sensors to calculate the air density and the coefficient K defined in Eq. (40), as done in Ref. [31]. Fig. 18 shows the convergence of the ATO at startup and after a current reference step. When initialized to zero, $\widehat{\theta}_e$ and $\widehat{\omega}_e$ provide correct estimations after 25 ms, even when the current i_q and the electric angular frequency ω_e are large and lead to an important difference between $\widehat{\theta}_e$ and $\widehat{\theta}_v - \pi/2$.

Table 1 presents the power provided to the load either by the diode-based rectifier or by the vector controlled switch-based AC/DC converter. In both cases, the proposed MPPT algorithm is used and the wind speed is constant. This table clearly evidences the higher efficiency of the second solution, as shown in §2.3. This particularly holds true at low speed.

We also tested the studied solutions with the quickly varying sinusoidal wind speed model used in Refs. [40,41].

$$V_w(t) = A_0 + \sum_{i=1}^{4} A_i \sin\left(\frac{2\pi t}{T_i}\right) \tag{43}$$

where the values of A_i and T_i are given in Appendix. Fig. 19 shows the results obtained with four different hardware and software solutions, including a diode-based rectifier associated to a boost circuit controlled by a Hill Climbing System (HCS) [16,40,42] used as MPPT algorithm. For this latter case, the setting of this algorithm was made difficult by the high inertia of our Darrieus wind turbine, which implies a very long sampling period (more than 15 s) to avoid stalling, as mentioned in Refs. [43,44]. The energy harvested during 100 s, 10203 J for the vector-controlled switch-based AC/DC converter using the proposed MPPT algorithm, 9886 J for the diode-based rectifier combined with a boost circuit using the proposed MPPT algorithm, 9754 J for the diode-based rectifier supplying a

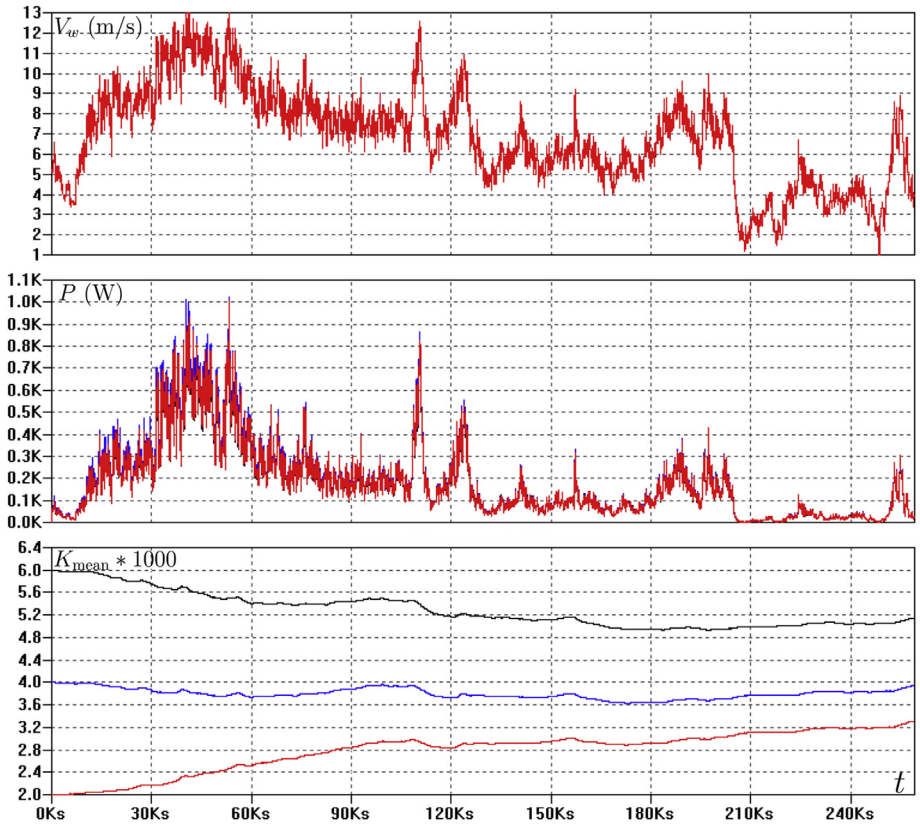

Fig. 20. Simulations results showing the K_{opt} evolution with the controlled rectifier when using a real wind speed data file recorded at Saint-Nazaire during 3 days. The K_{opt} behavior is observed for three initial values.

Table 2
Energy harvested during three days when using a constant K (case 1) or when using a maximum seeking process (case 2).

Initial $K_{mean}\times 1000$	Energy (1) (W.h)	Energy (2) (W.h)	Gain (%)	Final $K_{mean}\times 1000$
6	13025	13191	+1.3	5.15
4	13476	13427	−0.36	3.94
2	12377	12883	+4.1	3.31

resistive load matched to the average wind speed, and 7085 J for a diode-based rectifier combined with a boost circuit controlled by an HCS MPPT algorithm, clearly evidences the interest of the proposed solution.

Finally, Fig. 20 shows some simulation results obtained by the vector controlled switch-based AC/DC converter and the proposed MPPT algorithm with a real wind speed recorded between october 1st and october 3rd, 2010 by MeteoFrance, the french meteorology and weather forcasting agency. The energy harvested either with a fixed value of K or when using a maximum seeking algorithm is presented in Table 2 for different initial values of K. This table shows that when the initial value of K is correct (around 4), letting K evolve leads to a slight energy loss. But when the initial value of K is incorrect, the maximum seeking algorithm significantly improves the energy efficiency.

6. Conclusion

In this article, a consistent modeling of a complete wind energy conversion chain has been presented. This, unfortunately, is not very easy and not so widespread. A new Maximum Power Point Tracking algorithm has been designed, that permanently controls the duty cycle of a boost circuit or the i_{qref} of a controlled rectifier to maximize the power supplied to a DC load. An Angle Tracking Observer has been used to estimate the shaft speed and thus to maximize this power without using any mechanical sensor. The proposed algorithm neither requires a rotor speed sensor nor a wind velocity measurement. Simulations using LTspice have been used to demonstrate the performances of this method. This paper includes the comparison of the proposed wind energy conversion chain with another one using a three-phase inverter and a field oriented vector control. Further researches include the validation of these algorithms on an experimental prototype.

Acknowledgment

This work was partially supported by the French Région Pays de la Loire as part of the scientific program Aérojoules. The authors would like to thank Météo-France which allowed us to feed our simulations with real data recorded in Saint-Nazaire in 2010. Météo-France is a French public institution in charge of meteorology and weather forecasts.

Appendix. Model parameters

Wind model:		
$A_0 = 6$ m/s,	$A_1 = 0.2$ m/s	$T_1 = 60$ s
	$A_2 = 2$ m/s	$T_2 = 23.5$ s
	$A_3 = 1$ m/s	$T_3 = 4.8$ s
	$A_4 = 0.2$ m/s	$T_4 = 1.7$ s
Wind turbine: Darrieus vertical axis wind turbine:		
Radius		$R = 1.0$ m
Height		$H = 2$ m
$C_p(\lambda) = \sum_{k=0}^{4} C_k \lambda^k$	$C_0 = 0.110898$	$C_1 = -0.02493$
	$C_2 = 0.057456$	$C_3 = -0.01098$
	$C_4 = 0.00054$	
Shaft:		
Total inertia		$J = 5$ kg.m^2
Total friction coefficient		$f = 9.08\,10^{-3}$ N.m.s
Permanent magnet synchronous generator:		
Nominal power at 600 rpm		$P = 900$ W
Phase resistance		$R_s = 0.23\,\Omega$
Phase inductance		$L_d = L_q = 8$ mH
PM flux linkage amplitude		$\Phi_{sf} = 0.166$ Wb
Number of pole pairs		8
Line inductances		$L_{li} = 10$ mH
Current sensor impedance		$R_{sc} = 0.1\,\Omega$
Maximum power point tracking:		
Sinusoid amplitude		$a = 7\,10^{-4}$
Reactivity		$\varepsilon = 7\,10^{-11}$
Optimal value of K_{mean}		$K_{opt} = 4.066\,10^{-3}$
Angle tracking observer:		
Proportional gain		$K_a = 57$
Integral gain		$K_b = 214\,s^{-1}$
Load:		
Load resistance		$R_L = 150\,\Omega$

References

[1] M. Drugă, C. Nichita, G. Barakat, Performances study of direct coupled PM generator based small wind converters, in: Proc. IEEE ICEM, 2010.
[2] A. Mirecki, X. Roboam, F. Richardeau, Architecture complexity and energy efficiency of small wind turbines, IEEE Trans. Ind. Electron 54 (1) (2007) 660–670.
[3] S.O. Ani, H. Polinder, J.A. Ferreira, Comparison of energy yield of small wind turbines in low wind speed areas, IEEE Trans. Sustain. Energy 4 (1) (2013) 42–49.
[4] G. Moor, H. Beukes, Maximum power point trackers for wind turbines, in: IEEE Power Elect. Specialist Conf, 2004, pp. 2044–2049.
[5] J. Chen, J. Chen, C. Gong, Constant-bandwith maximum power point tracking strategy for variable-speed wind turbine and its design details, IEEE Trans. Indust. Elec 60 (11) (2013) 5050–5058.
[6] A. Mahdi, W. Tang, L. Jiang, Q. Wu, Comparative study on variable-speed operations of a wind generation system using vector control, in: ICREPQ, 2010.
[7] R. Esmaili, X. Longya, Sensorless control of permanent magnet generator in wind turbine application, in: Proc. IEEE IAS Conf, 2006, pp. 2070–2075.
[8] M. Andriollo, M. De Bortoli, G. Martinelli, A. Morini, A. Tortella, Control strategies for a VAWT driven PM synchronous generator, in: Proc. IEEE SPEEDAM, 2008, pp. 804–809.
[9] M.A. Abdullah, A.H.M. Yatim, C.W. Tan, R. Saidur, A review of maximum power point tracking algorithms for wind energy systems, Renew. Sustain. Energy Rev. 16 (2012) 3220–3227.
[10] S.M.R. Kazmi, H. Goto, H.J. Guo, O. Ichinokura, A novel algorithm for fast and efficient speed-sensorless maximum power point tracking in wind energy conversion systems, IEEE Trans. Indust. Elec 58 (1) (2011) 29–36.
[11] Z. Boulbair, M. Hilairet, F. Auger, L. Loron, Sensorless control of a PMSM using an efficient extended Kalman filter, in: Proc. IEEE ICEM, 2004.
[12] J. Thongam, P. Bouchard, H. Ezzaidi, M. Ouhrouche, Wind speed sensorless maximum power point tracking control of variable speed wind energy conversion systems, in: Proc. IEEE IEMDC, 2009, pp. 1832–1837.
[13] R. Aubrée, F. Auger, P. Dai, A new low-cost sensorless MPPT algorithm for small wind turbines, in: Proc. IEEE Int. Conf. On Renewable Energies and Vehicular Technology (REVET), Hammamet, Tunisia, 2012, pp. 305–311.
[14] J. Brahmi, L. Krichen, A. Ouali, A comparative study between three sensorless control strategies for PMSG in wind energy conversion system, Appl. Energy 86 (9) (2009) 1565–1573.
[15] A. Rolān, A. Luna, G. Vázquez, D. Aguilar, Modeling of a variable speed wind turbine with a permanent magnet synchronous generator, in: Proc. IEEE Int. Symp. On Indust. Electron. (ISIE'09), 2009, pp. 734–739.
[16] T. Tafticht, K. Agbossu, A. Chériti, DC bus control of variable speed wind turbine using a buck-boost converter, in: Proc. IEEE Power Engineering Society General Meeting, 2006.
[17] J. Hui, An Adaptive Control Algorithm for Maximum Power Point Tracking for Wind Energy Conversion Systems, Master's thesis, Queen's University, Kingston, Ontario, Canada, 2008.
[18] L.G. González, E. Figueres, G. Garcerá, O. Carranza, Synchronization techniques comparison for sensorless control applied to PMSG, in: ICREPQ Conf, 2009.
[19] E. Sambrata, J. Raharijaona, G. Barakat, B. Dakyo, Modeling and test of a PM synchronous generator based small stand-alone wind energy converter, in: Epe-ieee PEMC, 2006, pp. 1591–1596.
[20] D. Bertsekas, Constraiend Optimization and Lagrange Multipliers, Athena Scientific, 1996.
[21] S. Jiao, G. Hunter, V. Ramsden, D. Patterson, Control system design for a 20 kW wind turbine generator with a boost converter and battery bank load, in: Proc. IEEE PESC, 2001, pp. 2203–2206.
[22] C.T. Pan, Y.L. Juan, A novel sensorless MPPT controller for a high efficiency microscale wind power generation system, IEEE Trans. Energy Convers. 25 (1) (2010) 207–216.
[23] M. Mao, F. Liu, J. Mu, B. Xu, Sensorless control of PMSG for a wind power system based on CSC, in: Proc. IEEE ICPE-ecce, 2011.
[24] Y. Weizheng, K. Woo, Z. Ruijie, G. Wei, W. Yue, Analyze of current control strategy based on vector control for permanent-magnet synchronous generator in wind power system, in: Proc. IEEE IPEMC, 2009, pp. 2209–2212.
[25] F. Blaschke, The principle of field orientation as application to the new transvector closed-loop control system for rotating field machines, Siemens Rev. 34 (1972) 217–220.
[26] N. Quang, J. Dittrich, Vector Control of Three-phase AC Machines, Springer, Germany, 2008.
[27] Texas Instruments, Clarke and Park Transforms on the TMS320C2xC2xx, Application note BPRA 048, 1997.
[28] S. Vukosavic, Digital Control of Electrical Drives, Springer, 2006.
[29] M.E. Haque, M. Negnevitsky, K.M. Muttaqi, A novel control strategy for a variable-speed wind turbine with a permanent-magnet synchronous generator, IEEE Trans. Ind. Electron 46 (1) (2010) 331–339.
[30] J. Chen, J. Chen, C. Gong, New overall power control strategy for variable-speed fixed-pitch wind turbines within the whole wind velocity range, IEEE Trans. Indust. Elec 60 (7) (2013) 2652–2660.
[31] J. Thongam, M. Tarbouchi, R. Beguenane, A. Okou, A. Merabet, P. Bouchard, An optimum speed MPPT controller for variable speed PMSG wind energy conversion systems, in: Proc. IEEE IECON, 2012, pp. 4273–4277.
[32] Y. Tan, W. Moase, C. Manzie, D. Nesic, I. Mareels, Extremum seeking from 1922 to 2010, in: Proc. Of the 29th Chinese Control Conference, 2010, pp. 14–26.
[33] S. Bolognani, R. Petrella, A. Prearo, L. Sgarbossa, Automatic tracking of mtpa trajectory in ipm motor drives based on ac current injection, IEEE Trans. Ind. Appl. 47 (1) (2011) 105–114.
[34] I. Munteanu, A.I. Bratcu, E. Ceanga, Wind turbulence used as searching signal for MPPT in variable-speed wind energy conversion systems, Renew. Energy 34 (2009) 322–327.
[35] K. Tan, S. Islam, Optimum control strategies in energy conversion of PMSG wind turbine system without mechanical sensors, IEEE Trans. Energy Convers. 19 (2) (2004) 392–399.
[36] D. Nesic, Extremum Seeking Control: Convergence Analysis 15 (3–4) (2009) 331–347. Elsevier.
[37] A. El Magri, F. Giri, G. Besançon, A. El Fadili, L. Dugard, F.Z. Chaoui, Sensorless adaptive output feedback control of wind energy systems with PMS generators, Control Eng. Pract. 21 (2013) 530–543. ELSEVIER.
[38] F. Auger, O. Mansouri-Toudert, A. Chibah, Design of advanced resolver-to-digital converters, in: Proc. Electrimacs, 2011.
[39] LTspice IV High Performance Simulator and Schematic Capture, 2013. URL, http://www.linear.com/designtools/software/#LTspice.
[40] T. Pan, Z. Ji, Z. Jiang, Maximum power point tracking of wind energy conversion systems based on sliding mode extremum seeking control, in: IEEE Energy 2030 Conf, 2008, pp. 660–670.
[41] B. Sareni, A. Abdelli, X. Roboam, D.H. Tran, Model simplification and optimization of a passive wind turbine generator, Renew. Energy 34 (2009) 2640–2650.
[42] E. Koutroulis, K. Kalaitzakis, Design of a maximum power tracking system for wind-energy-conversion applications, IEEE Trans. Ind. Electron 53 (2) (2006) 486–494.
[43] R. Wai, C. Lin, Y. Chang, Novel maximum-power-extraction algorithm for PMSG wind generation system, IET Electr. Power Appl. 1 (2) (2007) 275–283.
[44] M. Naranaya, G.A. Putrus, M. Jovanovic, P.S. Leung, S. McDonald, Generic maximum power point tracking controller for small-scale wind turbines, Renew. Energy 44 (2012) 72–79.